SUPPLEMENTARY DATA

Rational engineering of a native hyperthermostable lactonase into a broad spectrum phosphotriesterase

Pauline Jacquet[1°], Julien Hiblot[1ǂ°], David Daudé[2°], Céline Bergonzi[1,3], Guillaume Gotthard[1], Nicholas Armstrong[1], Eric Chabrière[1#], Mikael Elias[3#]

1 - CNRS UMR 7278, IRD198, INSERM U1095, APHM, Institut Hospitalier Universitaire Méditerranée-Infection, Aix-Marseille Université, 19-21 Bd Jean Moulin 13005 Marseille, France.

2 - Gene&GreenTK, IHU Méditerranée Infection, 19-21 Bd Jean Moulin, 13005 Marseille, France

3 - University of Minnesota, Department of Biochemistry, Molecular Biology and Biophysics & Biotechnology Institute, St. Paul, MN 55108, USA

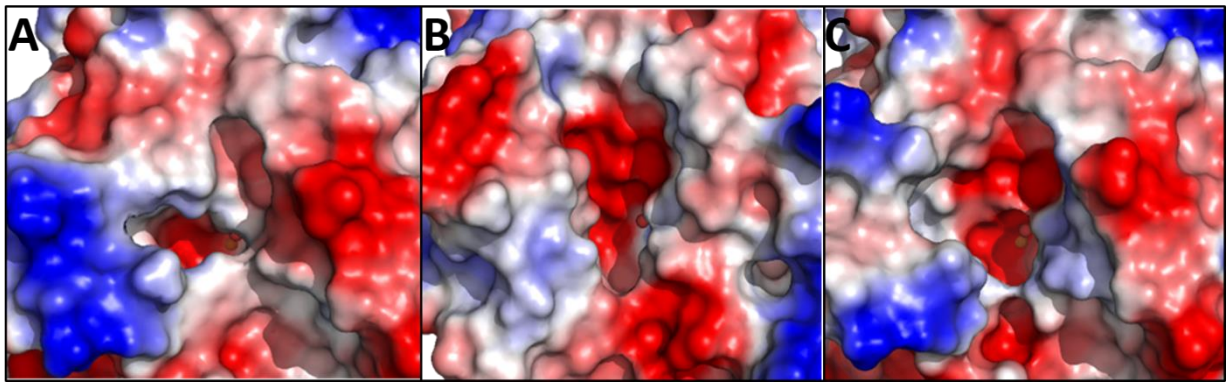

Figure S1: Structure-based active site cavity redesign. Active site cavity view of (**A**) *wt* *Sso*Pox, (**B**) *Bd*PTE and (**C**) *Sso*Pox modelled with all 14 designed mutations (Table S1). The mutations modelled were constructed *in silico* and energy was minimized using *Swiss PDB viewer*.[59] Electrostatic potentials were calculated using PyMOL[60] and are shown on the molecular surface. Electrostatic potentials are represented at the enzyme's surfaces. Blue, red and white indicates positively-, negatively-, and neutrally-charged areas, respectively.

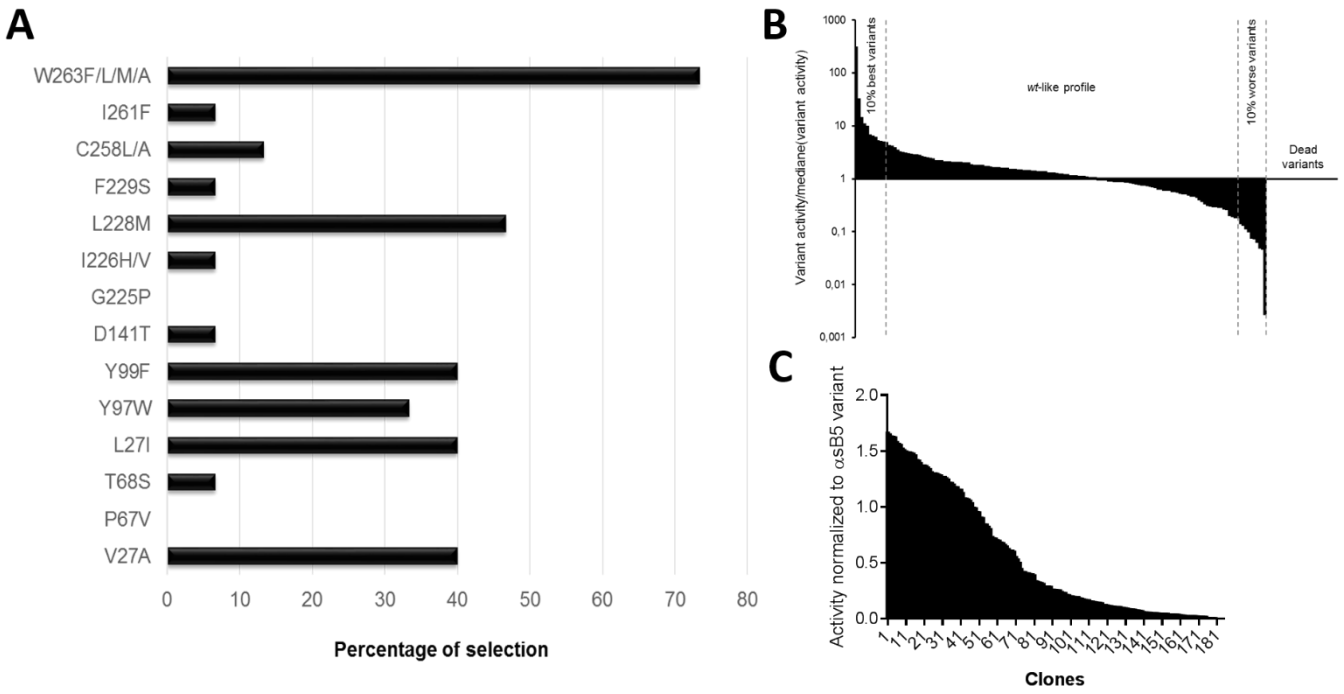

Figure S2: Library screening data. (**A**) Occurrence of mutations in the 14 best sequenced clones. (**B**) Screening profile of the combinatorial mutation library (184 clones) with paraoxon as a substrate. Activities (mOD_{405nm} min^{-1}) were normalized to the median value. (**C**) Screening of the position 263 saturation library (αsB5 background) with paraoxon as the substrate. Activity was normalized to αsB5 paraoxonase activity.

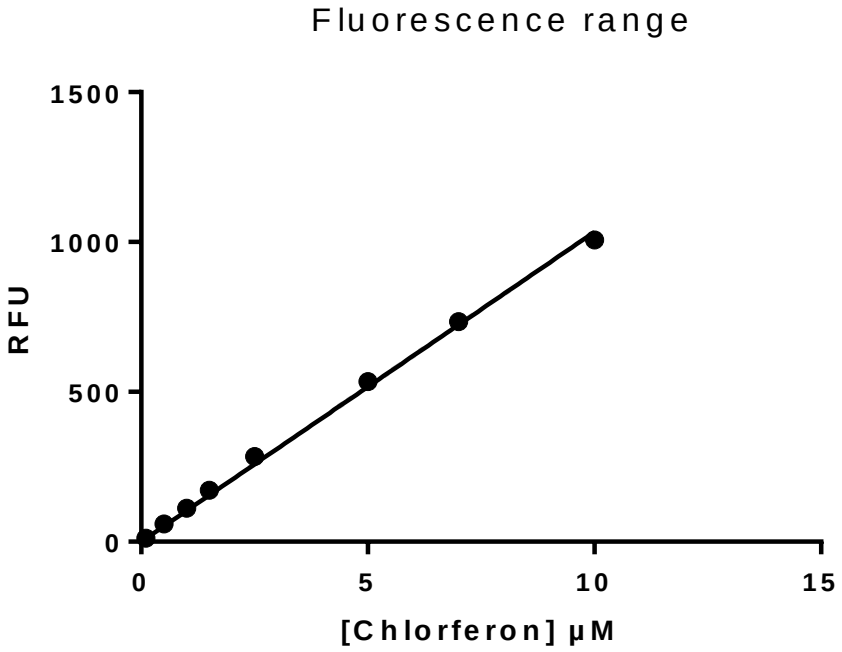

Best-fit values	
Slope	103,3 ± 0,6551
Equation	Y = 103,3*X - 0,0
R^2	0.9975

Figure S3. Chlorferon vs Fluorescence (360 (40) / 460 (40)) range of linearity

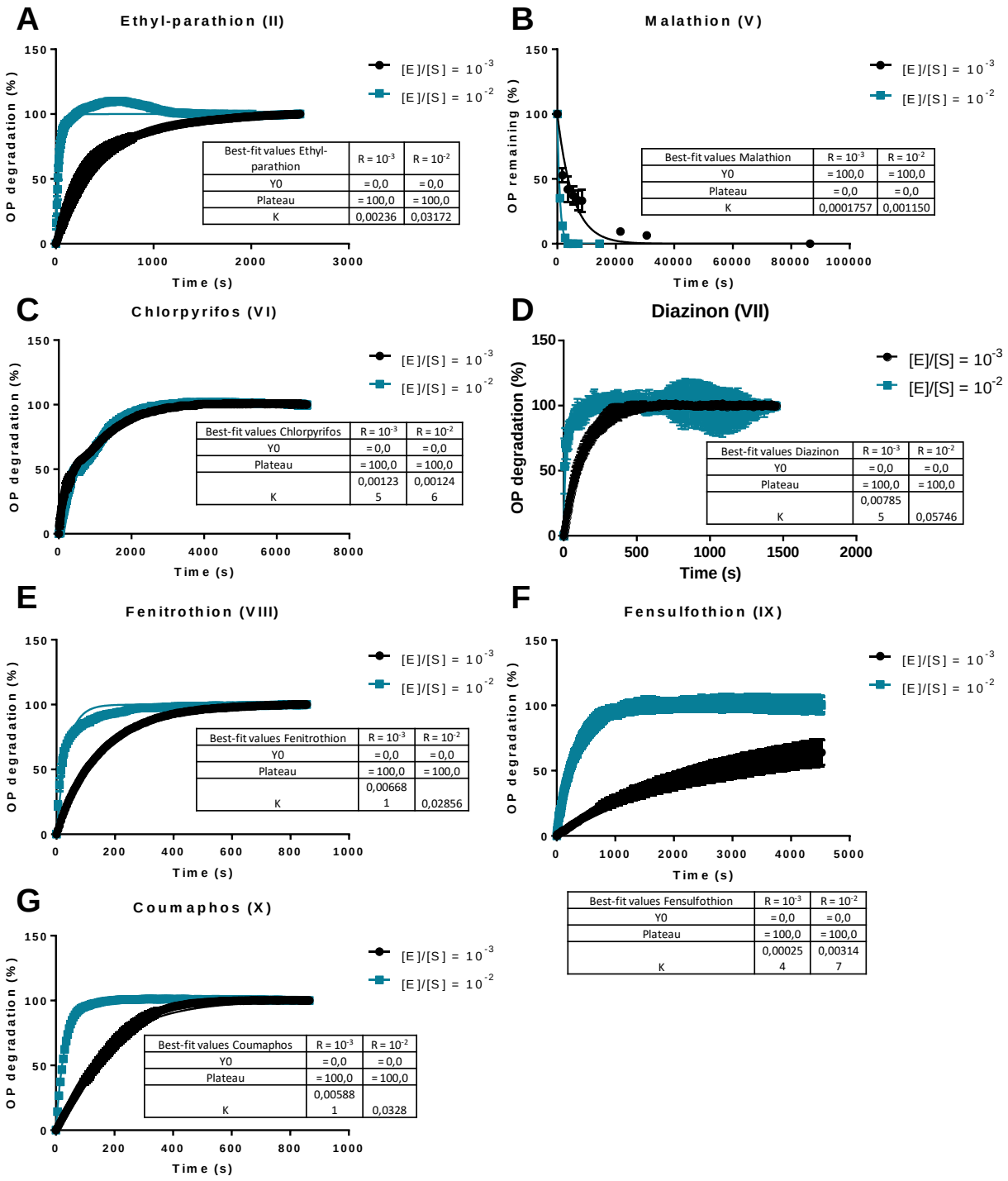

Figure S4. Bioremediation of organophosphorus insecticides (250 µM)

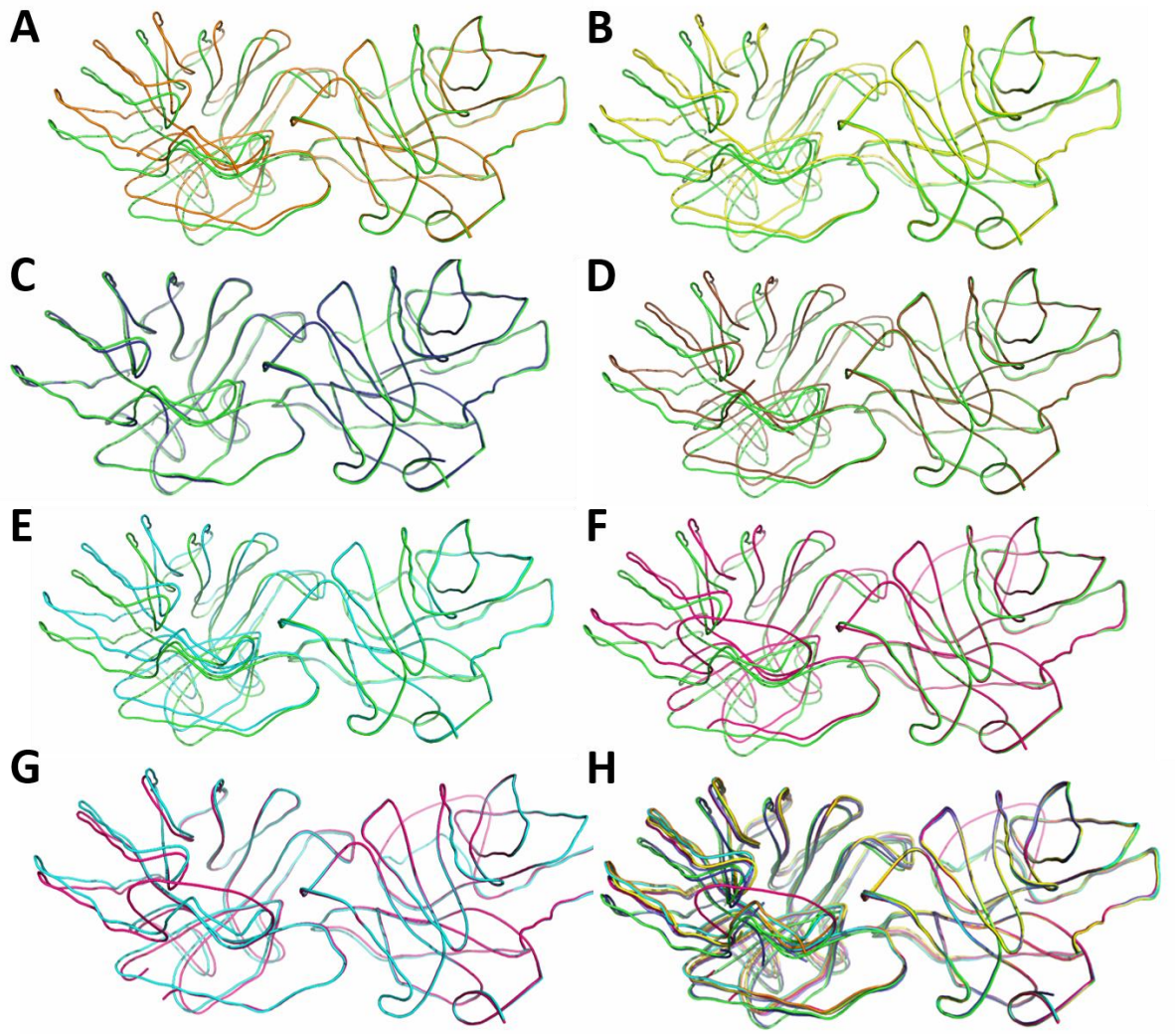

Figure S5. Structural superposition of wt-*Sso*Pox and mutants dimers. The monomers on the right were superimposed, and the difference with the left monomers indicates the relative reorientation of dimerized monomers. (**A**) Superposition of wt-*Sso*Pox (green) and αsA1 (orange). (**B**) Superposition of wt-*Sso*Pox (green) and αsB5 (yellow). (**C**) Superposition of wt-*Sso*Pox (green) and αsC6 (blue). (**D**) Superposition of wt-*Sso*Pox (green) and αsD6 (brown). (**E**) Superposition of wt-*Sso*Pox (green) and αsA6-CC (cyan). (**F**) Superposition of wt-*Sso*Pox (green) and αsA6-OC (magenta). (**G**) Superposition of αsA6-OC (magenta) and αsA6-CC (cyan). (**H**) Superposition of wt-*Sso*Pox (green), αsA1 (orange), αsB5 (yellow), αsD6 (brown), αsC6 (blue), αsA6-OC (magenta) and αsA6-CC (cyan).

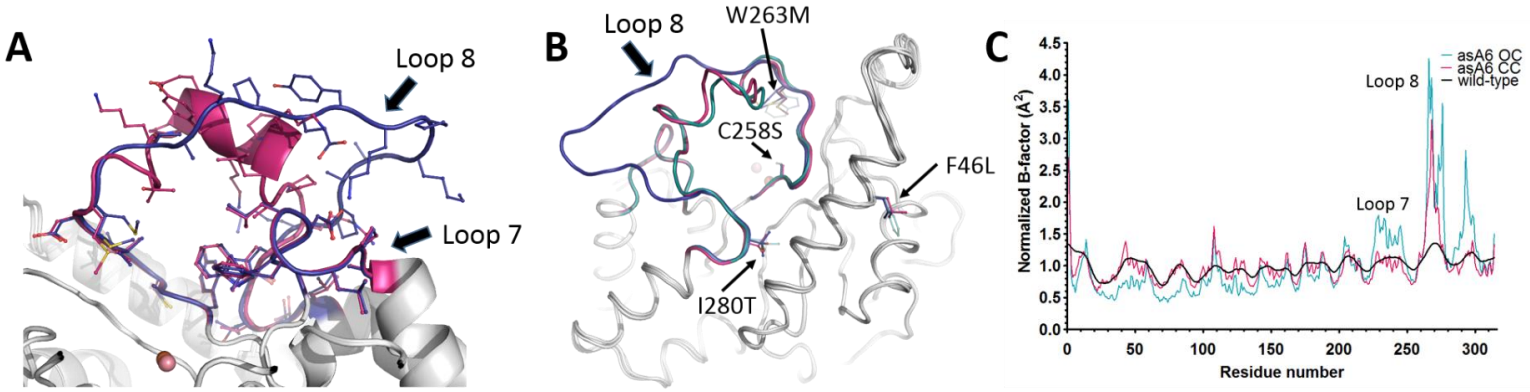

Figure S6. Mutant αsA6 loop-8 conformational flexibility. (**A**) Superposition of the open conformation (OC, blue) and the closed conformation (CC, magenta), of loop 8 in two distinct mutant αsA6 crystal structures. (**B**) Location of the four mutations of mutant αsA6 in the structure. The wt *Sso*Pox, the CC, and the OC loop 8 conformations are shown in green, magenta and blue, respectively. We note that I280T and C258S are located at the very beginning and end of loop 8. (**C**) Positional distributions of normalized B-factor values (the x-axis represents residue number) for wt-*Sso*Pox (black line), αsA6-OC (blue line) and (magenta line).

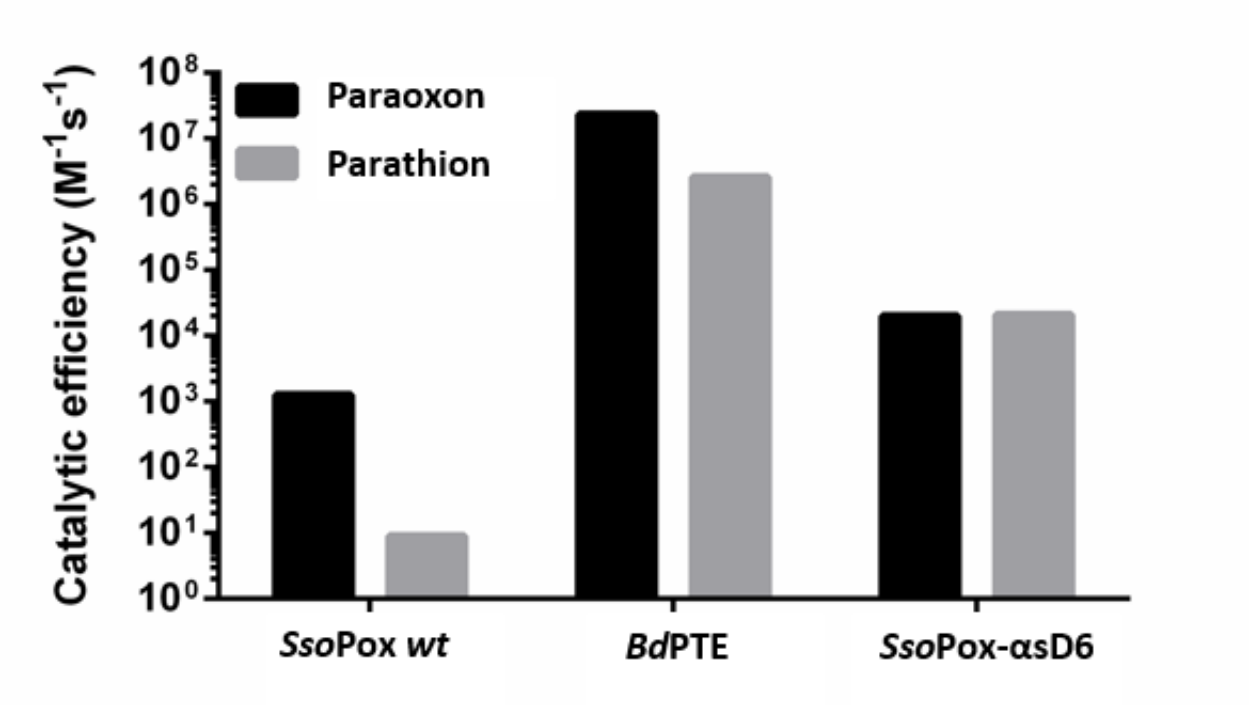

Figure S7: Thiono-effect in *Sso*Pox. Catalytic efficiencies of enzymes, *Sso*Pox, *Bd*PTE and *Sso*Pox-αsD6 with methyl-paraoxon (black) and methyl-parathion (gray) as substrates are shown.

Table S1: Mutation database

	*Sso*Pox posistion	Corresponding position in *Bd*PTE	Redesign	Additional mutations	Mutations in database
First set of mutations	V27	G60	-	-	V27A
	P67	V101	-	-	P67V
	T68	S102	-	-	T68S
	L72	I106	-	-	L72I
	Y97	W131	-	-	Y97W
	D141	T173	-	-	D141T
	G225	P256	-	-	G225P
	L226	H257	-	-	L226H
	C258	L303	-	A	C258/A-L
	I261	F306	-	-	I261F
Second set of mutations	Y99	-	F	-	Y99F
	L228	-	M	-	L228M
	F229	-	S	-	F229S
	W263	-	A	Saturation	W263/All

Table S2: Oligonucleotide sequences used in this study

Primer name			Primer sequence
Clonage	T7-prom		TAA TAC GAC TCA CTA TAG GG
	pET-RP		GCT AGT TAT TGC TCA GCG G
	SsoPox-lib-pET-5'		CAT GCC ATG GCG CGC ATT CCG CTG GTT GGT AAA G
	SsoPox-lib-pET-3'		AAG GAA AAA AGC GGC CGC TTA TTA GCT AAA GAA TTT TTT CGG ATT TTC
Primer name		**Encoding variation**	**Primer sequence**
Primers used in ISOR protocol	SP1	V27A	GAA CAT CTG CGT **GCA** TTT AGC GAA GCA GTT
	SP2	P67V-T68S	AAA ACC ATT GTT GAT **GTG AGT** GTT ATG GGT
	SP3	P67V	AAA ACC ATT GTT GAT **GTG** ACC GTT ATG GGT
	SP4	T68S	AAA ACC ATT GTT GAT CCG **AGT** GTT ATG GGT
	SP5	L72I	GTT ATG GGT **ATT** GGT CGT GAT ATT CGT TTT
	SP6	Y97W-Y99F	GGC ACC GGT ATT **TGG** ATT **TTT** ATC GAT CTG CCG
	SP7	Y97W	GGC ACC GGT ATT **TGG** ATT TAT ATC GAT CTG CCG
	SP8	Y99F	GGC ACC GGT ATT TAT ATT **TTT** ATC GAT CTG CCG
	SP9	D141T	AAA ATT GCA GCC **ACC** GAA CCG GGT ATT ACC
	SP10	L226H-228L/M-229F/S	GAT CGT TAT GGT **CAC** GAC **MTG TYT** CTG CCG GTT
	SP11	L226V-228L/M-229F/S	GAT CGT TAT GGT **GTG** GAC **MTG TYT** CTG CCG GTT
	SP12	G225P-228L/M-229F/S	GAT CGT TAT **CCG** CTG GAC **MTG TYT** CTG CCG GTT
	SP13	G225P-L226H-228L/M-229F/S	GAT CGT TAT **CCG CAC** GAC **MTG TYT** CTG CCG GTT
	SP14	G225P-L226V-228L/M-229F/S	GAT CGT TAT **CCG GTG** GAC **MTG TYT** CTG CCG GTT
	SP15	228L/M-229F/S	GAT CGT TAT GGT CTG GAC **MTG TYT** CTG CCG GTT
	SP16	C258L	ATT AGC CAT GAT TAT **CTG** TGC ACC ATT GAT
	SP17	C258A	ATT AGC CAT GAT TAT **GCC** TGC ACC ATT GAT
	SP18	I261F	GAT TAT TGC TGC ACC **TTT** GAT TGG GGC ACC
	SP19	W263F	TGC ACC ATT GAT **TTT** GGC ACC GCA AAA CCG
	SP20	W263M	TGC ACC ATT GAT **ATG** GGC ACC GCA AAA CCG
	SP21	W263L	TGC ACC ATT GAT **CTG** GGC ACC GCA AAA CCG
	SP22	W263A	TGC ACC ATT GAT **GCG** GGC ACC GCA AAA CCG

Table S3: Selected positions for phosphotriesterase activity improvement

Position	27	67	68	72	97	99	141	225	226	228	229	258	261	263	Additional	Total variations
wt	V	P	T	L	Y	Y	D	G	I	L	F	C	I	W		
B3	A			I	W					M						V27A/L72I/Y97W/L228M
F2										M				L		L228M/W263L
F8				I										M	K54I	K54I/L72I/W263M
B2	A			I		F	T			M				M	G7S/V28A	G7S/V27A/V83A/L72I/Y99F/D141T/L228M/W263M
H8			S		W	F				M						T68S/Y97W/Y99F/L228M/
E3	A			I										M	V83A/E173T	V27A/L72I/V83A/E173T/W263M
A4						F				M				M	G193S	Y99F/G193S/L228M/W263M
A1												L	F	A		C258L/I261F/W263A
A6												A		M	F46L/I280T	F46L/C258A/W263M/I280T
B5	A				W	F			V						I76T/L130P	V27A/I76T/Y97W/Y99F/L130P/L226V
C6				I		F				M	S			L	I122L	L72I/Y99F/I122L/L228M/F229S/W263L
D6	A				W					M				M		V27A/Y97W/L228M/W263M
D1					W											Y97W
D5				I										F		L72I/W263F
A5	A					F								L		V27A/L72I/Y99F/W263L
Incorporation	6	0	1	6	5	6	1	0	1	7	1	2	1	11		
Ratio	0.4	0	0.07	0.4	0.33	0.4	0.07	0	0.07	0.47	0.07	0.13	0.07	0.73		

Table S4: Tm values of *Sso*Pox variants

Enzyme	Mutations	T_m (°C)
wt	*	106
αsD6	V27A/Y97W/L228M/W263M	82.5 ± 1,8
αsB5	V27A/I76T/Y97W/Y99F/L130P/L226V	70.4 ± 3,1
αsB5 W263M	V27A/I76T/Y97W/Y99F/L130P/L226V/W263M	69.1 ± 2,3
αsB5 W263L	V27A/I76T/Y97W/Y99F/L130P/L226V/W263L	80.2 ± 4,0
αsB5 W263I	V27A/I76T/Y97W/Y99F/L130P/L226V/W263I	77.9 ± 1,3
W263M	W263M	85.3 ± 0,9
W263L	W263L	92.0 ± 2,1

Melting temperature determination. Circular Dichroism (CD) spectra were obtained using a Jasco J-815 CD spectrometer with a Pelletier-type temperature control system (Jasco MPTC-490S) in a 1 mm thick quartz Starna® cell and using Spectra Manager software. Experiments were carried out in 10 mM phosphate buffer at pH 8.0. Proteins concentrations were within 0.2–0.4 $mg.mL^{-1}$, denaturation was followed at 222 nm with temperature increased from 25 to 85°C (with $5°C.min^{-1}$ increment). A range of between 0.5 and 3 M of guanidinium chloride in 10 mM phosphate buffer at pH 8.0 was applied. Data were analyzed with GraphPad Prism 6 using Boltzmann sigmoidal equation, and T_m at 0 M of guanidinium chloride was then extrapolated by linear regression.

Thermal stability of the engineered variants

We measured the melting temperature of variants αsD6, αsB5, αsB5-W263L, αsB5-W263M and αsB5-W263I in this study while the T_m values of *wt*, W263M and W263L were previously reported (**Table S4**).[7] All variants showed decreased T_m values as compared to the wild-type enzyme. These values ranged from 69 °C to 92 °C for αsB5-W263M and W263L, respectively. As previously reported, the role of residue 263 is crucial for overall enzyme stability. The stability of mono-substituted variants was globally less affected than the αsD6 and αsB5 scaffolds. The latter's Tm value decreased by 36 °C as compared to *Sso*Pox-WT, while the addition of a mutation at position W263 to its background was not destabilizing, suggesting that their contribution to stability may be different. While the T_m values for the best variants have decreased, they remain very stable (e.g. αsD6 has a T_m of 82.5°C), as compared with their mesophilic counterparts ($T_{m,BdPTE}$=67°C).[61] Additionally, the expression level of the *Sso*Pox and its mutants were ≈100-150 $mg.l^{-1}_{culture,}$ a higher level than the *Bd*PTE (≈3 $mg.l^{-1}_{culture}$)and ≈50 $mg.l^{-1}_{culture}$ for the improved *Bd*PTE-S5 variant.[61]

Interestingly, the range of recognized substrate was broadened when thermostability decreased which is consistent with previous reports suggesting that mutations often increase activity at the cost of stability (**Figure 7**).[62,63]